Published 03/28/2017

doi:10.4271/2017-01-0718
saeeng.saejournals.org

# Investigation of Small Pilot Combustion in a Heavy-Duty Diesel Engine

Carlos Jorques Moreno and Ola Stenlaas
Scania CV AB

Per Tunestal
Lund University

## ABSTRACT

Factors influencing pilot-injection combustion were investigated using heat release analysis in a heavy-duty diesel engine fuelled with standard diesel fuel.

Combinations of pilot-injection parameters i.e. pilot start of injection, pilot mass, pilot-main injection separation, and rail pressure were studied for various operating conditions and combustion phases. An experiment was designed to investigate the factors influencing the combustion of the pilot. For improved injected fuel-mass accuracy, reference data for the injectors were measured in a spray rig prior to the engine experiments.

Results show that cycle-to-cycle variations and cylinder-to-cylinder variations influence pilot autoignition and the amount of heat released. Rail pressure and injected pilot mass affect the obtained variance depending on the chamber conditions. The obtained combustion modes (premixed, diffusive) of pilot combustion were found to be a function of the injected mass and rail pressure.

**CITATION:** Jorques Moreno, C., Stenlaas, O., and Tunestal, P., "Investigation of Small Pilot Combustion in a Heavy-Duty Diesel Engine," *SAE Int. J. Engines* 10(3):2017, doi:10.4271/2017-01-0718.

## INTRODUCTION

The increasingly stringent regulations on particulate matter (soot), oxides of nitrogen (NOx) and other emissions have driven major efforts in research on closed-loop control of internal combustion engines [1]. Closed-loop combustion control aims to regulate the engine close to optimal operating conditions and to reduce the effects of external disturbances and cycle-to-cycle variations [2]. Furthermore, these methods allow the use of low emission combustion modes such as HCCI [3] or PPC [4], for which external disturbances could yield unstable behaviour [5]. Even though only common rail diesel combustion is studied in this paper, similar methods can be used to counteract disturbances such as rail pressure variations, injection quantity variations, intake conditions, mixture composition, etc. that disturb the desired (optimal) combustion.

Closed-loop combustion controllers usually use in-cylinder piezo-resistive or piezo-electric sensors to measure the pressure in the combustion chamber [6]. The in-cylinder pressure signal is used to estimate heat release during combustion [7]. An appropriate control algorithm uses this information to adjust the fuel injection timing and other actuators to regulate the engine. Load, combustion phasing [7] and NOx formation [8] are some examples of controlled variables. By controlling them, cycle-to-cycle variations can be reduced [9].

Single injection schemes are not always sufficient to control combustion. The availability of fast piezo-electric injectors with common rail technology allows multi-injection strategies [1]. Multi-injection hardware provides new degrees of freedom in combustion control. One common multi-injection scheme is the use of pilot-main injection. The pilot-injection effect on main combustion and engine performance has been investigated in a number of articles [10, 11, 12, 13, 14, 15, 16, 17, 18, 19]. The previous work shows that pilot injection can be used to reduce combustion noise for improved comfort [20, 21, 22, 23] and, if properly optimized, it can reduce oxides of nitrogen and particle emissions [20,21,24] with only a small penalty on efficiency [25].

The combination of in-cycle control with multi-injection strategies has been applied to split main-injection schemes. The injection pattern is controlled in-cycle by adjusting the first injection duration, the start of injection of the following injection, and its duration [7]. A number of variables have been used as a feedback reference to split the main injection. Some examples are the heat release trajectory [7] and the NOx formation trajectory from a real-time virtual sensor [26].

The factors that influence autoignition of the pilot, the heat release and the accumulated heat release were investigated. The objective is to quantify the cycle-to-cycle and cylinder-to-cylinder variation as a function of the studied variables. The results are relevant in studying the possibilities of in-cycle control taking into account the pilot

injection influence on the main injection. The results provide the necessary background to design pilot-injection controllers as well as information on how the cycle-to-cycle and cylinder-to-cylinder variations of pilot combustion can be counteracted by controlling the start of main injection and main-injection duration.

## BACKGROUND

### *Diesel Combustion*

Figure 1 illustrates the combustion process of common rail diesel combustion. Diesel combustion can be separated into four phases [27]. The fuel is injected between the start of injection (SOI) and end of injection (EOI). The combustion phases can be distinguished from the heat release rate (HR): initial jet development (physical delay and chemical delay) when the fuel starts to vaporize (SOV); triggering autoignition or start of combustion (SOC), premixed combustion and diffusive combustion, also called mixing-controlled, until end of combustion (EOC).

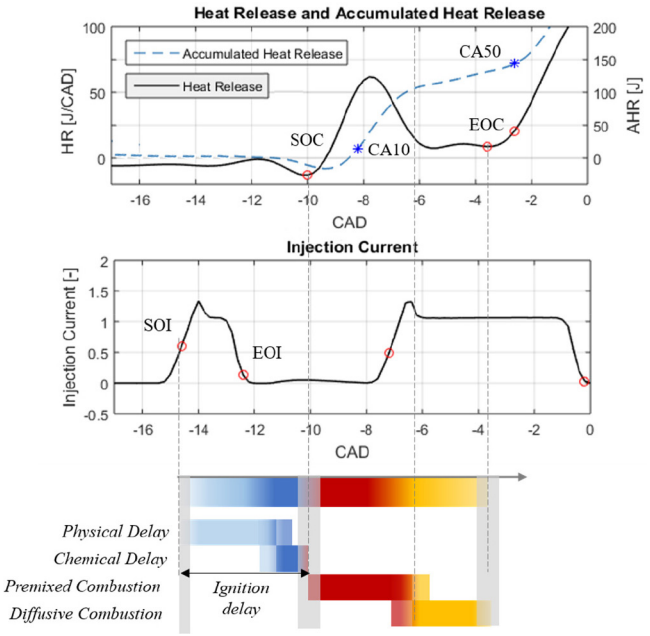


Figure 1. Heat release rate, accumulated heat release and pilot-injection traces at 1200rpm 10bar IMEP, -15CAD SOI pilot. The combustion phases are identified from the heat release. Identified combustion parameters are presented: Start of injection (SOI), start of combustion (SOC), end of injection (EOI), end of combustion (EOC), crank angle at 10%, 50% and 90% of the total heat release (CA10, CA50 and CA90). CA90 overlaps with main-injection heat release and is not plotted.

Physical delay consists of the time required for droplet break-up, air entrainment and vaporization. Even though fuel physical properties such as density, specific heat and volatility have an effect on the physical delay [28], with high pressure injection jets, the fuel injection pressure has a deterministic impact on the spray break-up and vaporization [29].

Chemical delay is controlled by the fuel's autoignition kinetics. This is dependent on fuel chemical composition, molecular structure and associated reactivity. Hence, pressure, charge temperature and local equivalence ratio conditions affect chemical ignition delay [28].

Physical delay and chemical delay usually overlap in time [27,30]. For compression ignition engines, physical delay is much longer than chemical delay [31]. The chamber conditions at SOI influence the duration of the physical and chemical processes [32]. Higher temperature reduces both delays: the higher thermal energy entrainment for the same mass of air speeds up the vaporization [33]. In addition, the chemical kinetics are faster and the chemical delay is shorter [34].

The chamber conditions also affect the chemical reactions that result in NOx and soot emissions [27,35].

## PREVIOUS WORK

Previous investigations on pilot injection explain its effect on main injection in the following way [16,18,19,25]: pilot injection modifies the mixture and chamber conditions by the start of main injection. The new chamber thermodynamic conditions are a result of pilot combustion and the heat released. Results in [15] show that pilot-injection timing has an effect on the amount of heat released for the same pilot injected mass. The more heat released from pilot injection, the higher the chamber temperature resulting in a reduction in main-injection ignition delay. Higher load and engine speed both benefit pilot combustion due to a higher pressure and temperature in the combustion chamber.

## EXPERIMENTAL SETUP AND METHOD

### *Engine Setup*

A modified Scania D13 heavy duty engine was used to perform the experiments. These modifications could mean that the results could be different to those obtained with a production engine. The geometrical specifications are listed in Table 1. The engine setup is illustrated in Figure 2.

Table 1. Engine Specification.

| | |
|---|---|
| Cylinder number | 6 |
| Displaced volume | 12.74 L |
| Stroke | 160 mm |
| Bore | 130 mm |
| Compression ratio | 18:1 |
| Number of Valves | 4 |
| Intake Valve Closing timing (IVC) | -151 CAD ATDC |
| Exhaust Valve Opening timing (EVO) | 146 CAD ATDC |

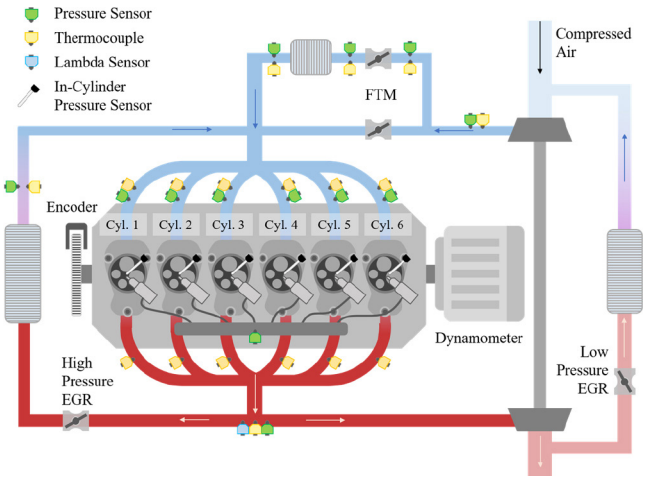


Figure 2. Engine Setup used in the experiment.

Engine speed is kept constant by the dynamometer, a 355kW AC motor, which also operated as an engine brake.

A Fast Thermal Management (FTM) system can be used to control the intake charge temperature through two regulated throttles, a hot and a cold with a cooler. The advantage is that the total cross-section can be kept constant to minimize the pressure loss. Low-pressure and high-pressure EGR are controlled from two regulated ball valves. No EGR was used in the experiments in this paper. An OEM turbocharger with wastegate is installed with the wastegate always closed. The engine is supplied with compressed air at a controlled pressure.

## *Sensor and Emission System*

A Leine-Linde crank angle encoder with 0.2 CAD resolution was used.

Inlet manifold and exhaust pressures were measured using Keller PAA-23S absolute pressure sensors. K-type thermocouples were used to measure inlet manifold and exhaust temperatures.

The cylinder pressure was measured using six water-cooled Kistler (7061B) in-cylinder pressure sensors. A torque sensor (T40B) from HBM measured the engine brake torque after the fly-wheel.

Fuel mass flow was measured using a mini CORI-FLOWTM M15 Mass Flow Meter from Bronkhorst with 10Hz sampling frequency. A Horiba MEXA-9100E was used to measure UHC, CO, $CO_2$ and NOx. An AVL Micro Soot Sensor was used to measure soot concentration.

## *Engine Control System*

The engine controller uses LabVIEW™ from National Instruments and NI hardware with a PXI chassis (NI PXIe-8135 2.3 GHz quad-core processor). The user interface was run on a PC with Windows 7 communicating with the real-time system over TCP/IP.

The real-time system consisted of two FPGA boards NI PXI-7854/7854 R (Multifunction reconfigurable I/O with Virtex 5-LX110/LX30 FPGA). The FPGA was used as flexible reconfigurable AO/DIO hardware for AD acquisition, triggered by the crank-angle encoder. The ADC resolution was 16-bits.

For the injectors and common rail pressure, external drivers from Drivven were used to execute the control action which was sent from the PXI system and commanded from the PC.

## *Combustion Control*

For pilot injection, measured reference data were used to create maps for which the injection on-time for different rail pressures is used to inject the commanded masses.

For the main injection, two PI controllers were used. One controlled the IMEP of the cylinder by controlling the injection duration. The fuel mass injected during main injection was estimated using the maps of the injectors.

The second PI controlled the CA50 position by defining the start of main injection. The CA50 reference was set by placing the HR-peak from the CAD from the experiment design.

CA50 and HRR peak were obtained from online heat release analysis implemented in LabVIEW™. The implemented HR algorithm was a simplified version of the one used in the analysis of the results.

## *Calibration of the Pilot Mass Injection*

To estimate the injected pilot mass, data were collected in a spray rig for each of the six injectors. The transfer function from the injectors on-time to the injected mass was calibrated. The threshold in the current trace for estimating the SOI and EOI was selected so that the mass estimated agreed with the transfer function and the values measured in the spray rig.

The pilot injection generates rail pressure oscillations that can influence the main injection. The oscillations from a second injection do not affect the pilot, but they can originate from a different injector. For this reason, even though the injected mass was measured for single injections, an additional method was used to estimate the mass for double injections. The injected mass was estimated from lambda measurements with a stoichiometric balance. The results were compared for single and multiple injections. Both methods gave the same result for estimation of the injected mass.

## Heat Release Analysis

In this paper, heat release analysis is according to the previous work presented by Tunestål in [36] and Johansson [37]. The method described in [38] is used to estimate the offset of the top dead centre (TDC). For the heat transfer, the adopted model is Woschni's [39].

The combustion parameters used are presented in Figure 1. The following definitions apply:

- **Start of injection (SOI)** is when the injector opens. It is estimated from the injection current at a calibrated threshold where mass estimated by the difference between SOI and EOI i.e. injection duration, agrees with measurements of injected mass in a spray rig. The threshold was set at half of the level of injection current at steady open state.
- **End of injection (EOI)** is when the injector closes. It is estimated from the injection current as done for the SOI. The threshold was set at 0.05 of the steady current.
- **CAx** is the required crank angle degrees (CAD) to complete the fraction X of the maximum accumulated heat released.
- **Start of combustion (SOC)** is the crank angle at which the first chemical energy is released. Different algorithms have been developed for on-line computation of SOC [40]. These algorithms use in-cylinder pressure measurements [41,42] or the heat release rate [43,44]. The latter approach is used in this paper as performed in [34,45]. A good trade-off between detectability and accuracy was found by placing SOC when the HR derivative is above a threshold of 18 J/CAD$^2$ after the minimum found after the main SOI, i.e. between SOV and SOC, see Figure 1.
- **End of combustion (EOC)** is the point at which the accumulated heat release (AHR) reaches 95% of its maximum.

## Experimental method

To investigate the effects of small pilot injections, three different variables were investigated for a combination of operating conditions:

a. Rail pressure
b. Pilot start of injection
c. Injected pilot mass

The experiment produces a central point test matrix. For 1200rpm, loads ranging between 2.5 to 15bar IMEP were studied in increments of 2.5bar IMEP. For 10 bar IMEP, engine speeds ranging from 600 to 1800 rpm were studied in increments of 300rpm. All combinations of variables were studied at the central point. To complete the experiment and study the interaction between engine speed and load, data was acquired for low engine speeds at low load, and for high engine speeds at high loads. The combinations of variables in those cases were reduced to avoid exponential growth of the number of data points. In total, 26 different operating points were studied (Table 2).

The operating conditions are listed in Table 3 which presents a summary of the combinations of variables studied for each operating condition.

Table 2. Operating conditions for each experimental case.

| **Engine Speed (RPM)** | **Engine Load (IMEP, bar)** | | | | | | |
|---|---|---|---|---|---|---|---|
| | **Motoring** | **2.5** | **5** | **7.5** | **10** | **12.5** | **15** |
| **600** | #1 | #6 | #9 | #12 | #16 | | |
| **900** | #2 | #7 | #10 | #13 | #17 | | |
| **1200** | #3 | #8 | #11 | #14 | #18 | #21 | #24 |
| **1500** | #4 | | | #15 | #19 | #22 | #25 |
| **1800** | #5 | | | | #20 | #23 | #26 |

Table 3. Combinations of variables for each experimental case.

| Case Number | Rail Pressure (bar) | CAD at Maximum HRR | Pilot Separation (CAD) | Pilot Mass (mg) |
|---|---|---|---|---|
| #6, #7 | 900 | 5 | 7.5, 10 | 0, 8, 10, 12 |
| #8 | 900, 1050 | 0, 5, 10 | 5, 7.5, 10 | 0, 6, 8, 10, 12 |
| #9, #10 | 900, 1050 | 0,5 | 7.5, 10 | 0, 8, 10, 12 |
| #11 | 1050, 1200 | 0, 5, 10 | 5, 7.5, 10 | 0, 6, 8, 10, 12 |
| #12 | 1050 | 0,5 | 7.5, 10 | 0, 8, 10, 12 |
| #13 | 900, 1050, 1200 | 0, 5 | 5, 7.5, 10 | 0, 8, 10, 12 |
| #14 | 1050 | 0, 5, 10 | 5, 7.5, 10 | 0, 6, 8, 10, 12 |
| #15 | 1050 | 5, 10 | 7.5, 10 | 0, 8, 10, 12 |
| #16 | 1200 | 0, 5 | 5, 7.5, 10 | 0, 8, 10, 12, 14 |
| #17, #19 | 1200 | 0, 5, 10 | 5, 7.5, 10 | 0, 6, 8, 10, 12 |
| #18 | 900, 1050 | 0, 5, 10 | 5, 7.5, 10 | 0, 6, 8, 10, 12 |
| | 900, 1050, 1200 | 5 | 7.5 | 0, 6, 7, 8, 9, 10, 12 |
| #20 | 1200 | 5, 10 | 5, 7.5, 10 | 0, 6, 8, 10, 12 |
| #21 | 1350 | 0, 5, 10 | 5, 7.5, 10 | 0, 8, 10, 12, 14 |
| #22, #23 | 1350 | 5, 10 | 7.5, 10 | 0, 9, 12, 15 |
| #24 | 1500 | 0, 5, 10 | 5, 7.5, 10 | 0, 8, 10, 12, 14 |
| #25, #26 | 1500 | 5, 10 | 7.5, 10 | 0, 9, 12, 15 |

Prior to the experiment, the engine was run for at least 30 min to ensure completely warmed-up conditions. When changing operating conditions and variable set-points, the engine was run for a minimum of 500 cycles until stationary conditions were reached. For each working condition and variable combination, data was logged for 200 cycles.

The fuel used for the experiment was standard Swedish Diesel fuel without RME.

# RESULTS AND DISCUSSION

## *Pilot Injection Uncertainty*

The studied pilot-injection masses are in the range of 6 mg/st to 15 mg/st. The short on-time required to supply these small amounts is sensitive to external factors which disturb the actual injected mass. As summarized in [28,46], these are: rail pressure offset, rail pressure oscillations, injection-to-injection variations due to dynamic injector behaviour and pressure difference along the injector [27,33,47], fuel viscosity and temperature [30,48].

Reference data was obtained in static conditions with a stable and constant pressure difference between intake and tip of the injector. For a constant reference on-time corresponding to 6 mg/st delivery, the obtained pilot mass was within 6±2 mg/st. The region of the injector characteristic on-time mass is non-linear and sensitive at low injection masses. When the pilot injection mass is too small, autoignition is not triggered, necessitating injection of the pilot using a detection method other than HR.

To confirm the opening of the injector for pilot masses under 8mg/st, a study was performed at 1200 rpm and 10 bar IMEP. The pilot injection was turned off for one cylinder at a time, sequentially every 50 cycles. This ensures that chamber conditions are the same for pilot-main and single injection. SOI of main injection was kept at the same CAD. The studied rail pressures were 900bar, 1050bar and 1200bar.

The accumulated heat release can be used to observe whether the combustion of the pilot injection is triggered and to corroborate that the pilot has been injected. The accumulated heat release from pilot injection as a function of the injected pilot mass is plotted for the six cylinders in Figure 3.

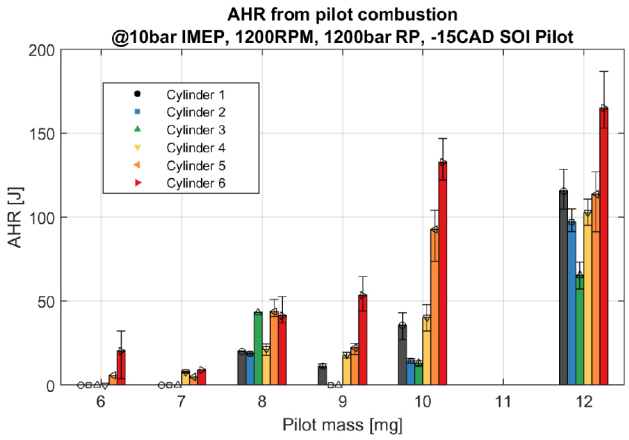


Figure 3. Accumulated heat release from combustion of the pilot-injection as a function of pilot-injection mass at 10bar IMEP, 12000rpm, 1200bar rail pressure and -15CAD SOI pilot. Bars represent one standard deviation of the data set within 200 cycles.

It is observed that the differences between the cylinders is highly significant which makes it is hard to establish a common relationship between the pilot mass and the AHR for all the cylinders. However, selecting one of the cylinders, it can be seen that for sufficiently large pilot masses i.e. large enough to trigger autoignition of the pilot, the AHR increases as the pilot mass is increased. For small masses, less than 9mg/st, the small HR makes it difficult to identify the SOC and therefore, for some cylinders, the AHR is greater for smaller masses.

The percentage of cycles when pilot-injection autoignition is triggered is presented in Figure 4. For increasing injected pilot mass, pilot ignition becomes more robust and more cycles burn. The minimum pilot-injection mass to ensure pilot ignition for all the cycles depends on the injector and the rail pressure, 1200bar in this case.

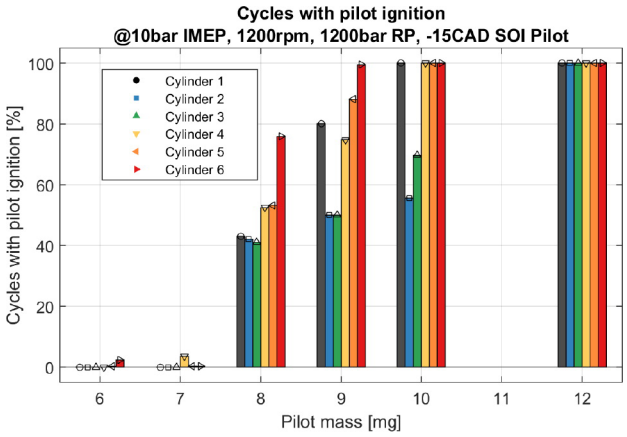


Figure 4. Percentage of cycles with pilot autoignition as a function of pilot-injection mass at 10bar IMEP, 12000rpm, 1200bar rail pressure and -15CAD SOI pilot.

In the cases of Figure 3 and Figure 4, the results are for a rail pressure of 1200bar. The AHR values lie within a wide range making it even more difficult to determine whether autoignition of the pilot injection is triggered for pilot masses over 6mg/st. The comparison can be done from the plot in Figure 5. Only the AHR of Cylinder 1 is plotted, for legibility. To illustrate the range of variation within the cylinders, the bars show the maximum and minimum variation within the cylinders.

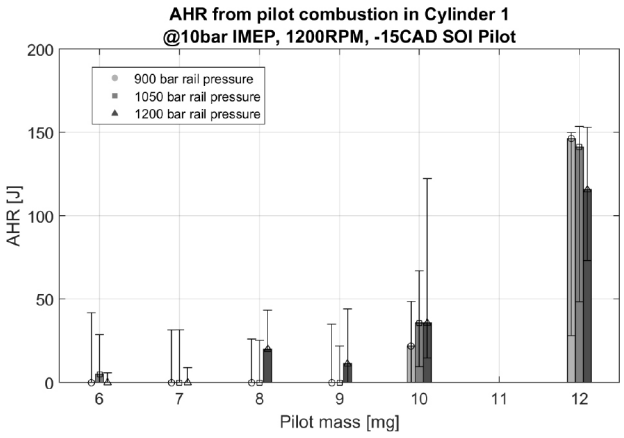


Figure 5. Accumulated heat release from combustion of the pilot-injection in Cylinder 1 as a function of pilot-injection mass at 10bar IMEP, 12000rpm and -15CAD SOI pilot. Bars represent the range of variation of for the six cylinders and the 200 cycles.

Heat release analysis is not sufficient for detection if the pilot is injected with masses under 8 mg/st. The difference in the in-cylinder rail pressure at SOI of main injection between cycles when the pilot was injected and when it was not, was analysed but did not give conclusive results, neither did the heat release analysis. Neither was it possible to obtain conclusive results from analysis of hydrocarbon emissions or lambda.

Therefore, the approach to verify that the pilot was actually injected for masses over 6mg/st used analysis of the pressure rise rate. Figure 6 presents the difference in the maximum pressure rise rate between cycles with pilot injection and without pilot injection.

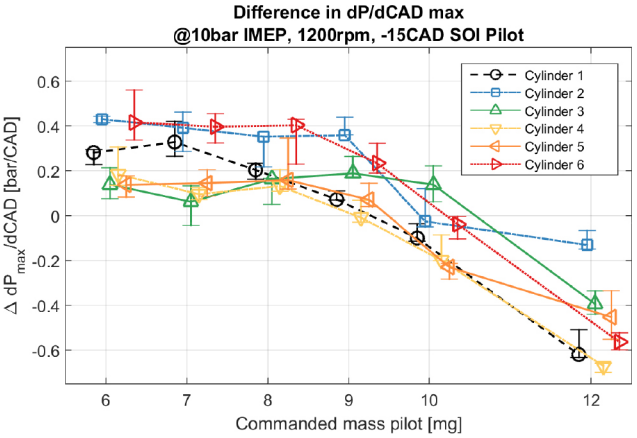


Figure 6. Difference in maximum pressure rise rate between cycles with pilot-injection and without as a function of commanded pilot mass for 1200bar rail pressure. Bars represent one standard deviation of the data set.

For small pilot masses, where pilot injection does not ignite (see Figure 4), there is an increase in the maximum pressure rise rate. The additional injected mass from the pilot increases the amount of premixed fuel, and does not reduce the main-injection ignition delay sufficiently to counteract this effect. When pilot injection ignites (over 9 mg/st for this operating condition) the maximum pressure rise rate is reduced. This can be explained by reductions in main-injection ignition delay and premixed combustion due to pilot heat release. Additional experiments would be necessary to confirm this. Individual lambda sensors mounted in each exhaust port were neither accurate nor fast enough to distinguish between single and pilot-main injection. Neither was the rail pressure drop due to the small pilot quantity. From these results, the pilot is assumed to be injected for all cylinders and for commanded masses over 6 mg/st for all studied rail pressures.

To determine which factors affect pilot-injection autoignition, the effect of rail pressure for 8mg/st pilot-injection mass at 7.5 and 10 bar IMEP, 900 and 1200 rpm is shown in Figure 7. For higher rail pressures, on-time is shorter and therefore more sensitive. Despite higher sensitivity, higher rail pressure increases spray penetration [49]. The longer spray penetration improves air entrainment, mixing and vaporization, which triggers pilot-injection autoignition [50]. 8mg/st pilot injection at -12.5CAD SOI ignites only at 1200 rpm, for rail pressures over 900 bar. For Cylinders 5 and 2, some cycles also burn at 900 bar rail pressure. The conclusion from this result is that mixing as well as chamber temperature are important to trigger pilot ignition (see Figure 8).

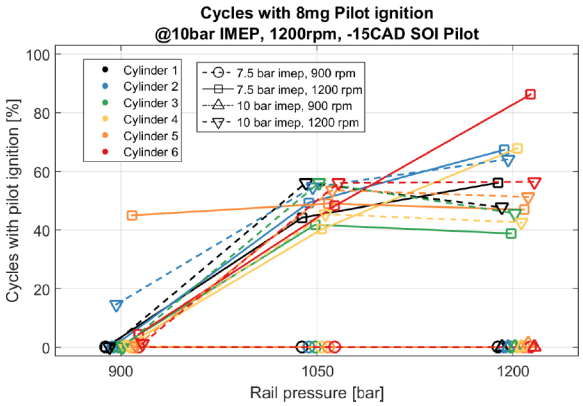


Figure 7. Percentage of cycles with pilot-injection autoignition versus rail pressure for 8mg/st commanded pilot at -15CAD SOI.

The next question is how the start of pilot injection affects the robustness of pilot autoignition. In Figure 8, the percentage of cycles when pilot injection ignites is presented as a function of the SOI of 8 mg/st pilot injection at 7.5 bar IMEP and 900 rpm. There is a clear trend that with later injection, pilot-injection autoignition is more robust. The chamber temperature is higher for later injection due to the thermodynamic state of the mixture. This facilitates pilot-injection autoignition. Previous discussions have shown that engine speed is also important. Higher engine speeds give a higher temperature due to higher friction and higher power. As apparent from the results in Figure 7, the consequence is a more robust pilot-injection ignition.

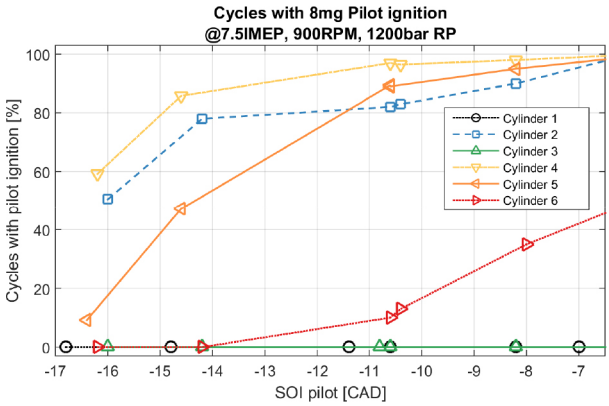


Figure 8. Percentage of cycles with pilot combustion as function of SOI, for 8mg/st commanded pilot at 1200bar rail pressure, 900rpm and 7.5bar IMEP.

It is worth noting that the pilot of cylinders 1 and 3 does not autoignite under these operating conditions despite the SOI. This is believed to be due to the actual injected mass being smaller than 8mg/st, together with the low thermal load. Even if autoignition is triggered, the very small effect on the HR makes it difficult for the algorithm to identify the SOC. A higher load and engine speed triggered autoignition of the 8mg/st pilot.

The pilot autoignition is different for each cylinder. The question remains about the cross-correlation of cycles when the pilot does not ignite for the different cylinders: is it the common operating conditions that determine a non-burning cycle, or is it the individual cylinder conditions? The cross-correlation within the cylinders for the cycles when the pilot autoignites was analysed; the results are presented in Figure 9 for Cylinder 1.

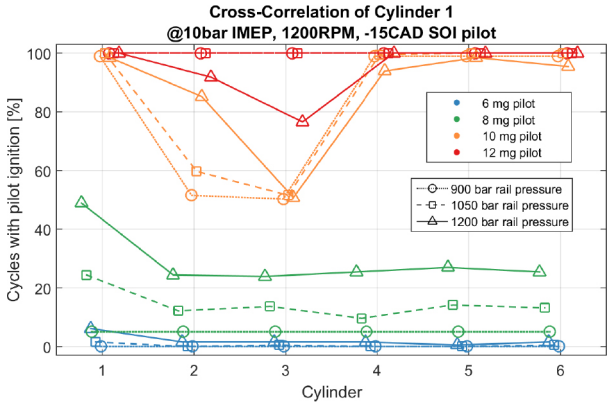


Figure 9. Cross-correlation of cycles with pilot autoignition for Cylinder 1 versus rail pressure and injected pilot mass at 10bar IMEP, 1200rpm and -15CAD pilot SOI.

For each pilot mass and rail pressure on the x-axis for Cylinder 1, the corresponding y-axis value is its auto-correlation, i.e. the percentage of cycles when the pilot autoignites for Cylinder 1. For the remainder of the cylinders on the x-axis, the y-axis value is the cross-correlation between Cylinder 1 and each other cylinder i.e. the percentage of cycles when there is pilot autoignition in Cylinder 1 and the other cylinder.

For 6mg/st pilot injection mass, there is no autoignition for most of the cycles regardless of the rail pressure. For 8mg/st pilot injection, around 50% of the cycles in Cylinder 1 give pilot autoignition at 1200bar rail pressure, giving a lower percentage as rail pressure decreases (see Figure 7). Comparing whether pilot autoignition was obtained for the same cycle as the rest of the cylinders, the results indicate that around 25% of those cycles did not ignite. The remaining 25% of the cycles that do not autoignite are a consequence of the individual cylinder conditions and variances in the actual injected pilot mass.

For 10mg/st pilot injection, the pilot auto-ignites for 99% of the cycles, but for Cylinder 3 only 50% of the cycles achieve pilot autoignition. This may be due to a smaller injection mass than the commanded 10mg/st for the injector in Cylinder 3, but would need to be confirmed by re-calibrating the injector. Similar results are seen with 12mg pilot injection mass. At a higher pilot mass, the effect of the individual cylinder conditions and pilot injection on the spread of pilot autoignition is reduced.

## *Combustion of Pilot Injection*

In this section, the phases and heat release of pilot-injection combustion are discussed as a function of the studied parameters. Pilot injection is comprised of the ignition delay, premixed combustion and diffusive combustion presented in Figure 1. These phases can be identified from the heat release rate trace. Injection parameters are identified from the injection current trace (SOI, EOI), from which HR, SOC and EOC can be identified. The AHR before main injection is used to determine CA10, CA50 and CA90. Note that the pilot-injection heat release overlaps with main injection for this injection separation. In this paper, end of pilot combustion is estimated as the crank angle at which 90% of pilot chemical energy is burned, or at SOC of main-injection if it is not reached before main-injection SOC (see Figure 1).

The accumulated heat release from pilot-injection at -15CAD SOI is presented in Figure 10 different loads at 1200rpm and different engine speeds at 10bar IMEP. Results show that accumulated pilot heat release increases with pilot-injection mass. The increase is nonlinear: a larger fraction of the pilot fuel energy is released with increasing pilot injected mass.

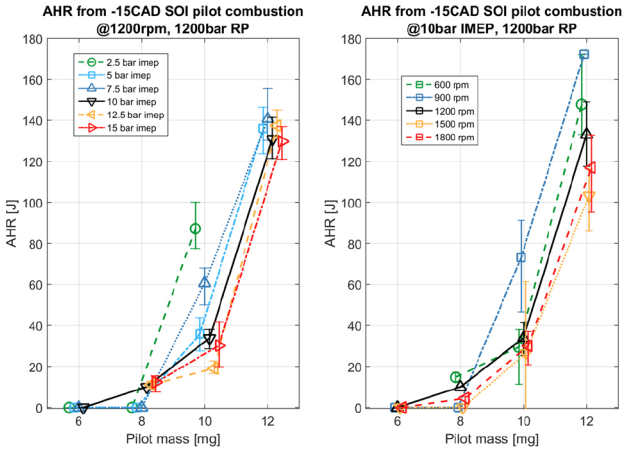


Figure 10. Accumulated heat release for different loads at 1200rpm (left) and for different engine speeds at 10bar IMEP (right); as a function of pilot-injection mass. Bars represent one standard deviation of the data set.

The same trend is obtained for the different engine speeds. At lower engine speeds, there is more available time before main injection for a constant separation between the injections. Therefore, the total AHR from pilot injection increases. However, the highest is obtained at 900rpm. This contradictory result is due to the fact that pilot ignition delay is also longer at 600rpm, which reduces the total available time.

The pilot-injection parameters EOI, SOC, CA10, CA50 and CA90 after SOI are presented in Figure 11 at 10bar IMEP and 1200rpm for pilot SOI at -15CAD. The effect of the abovementioned increase in the AHR due to the larger injected pilot mass is observed as an advance in SOC. The higher HR does not retard CA50 and CA90 to any great extent. From heat release analysis, it was observed that up to 60% of the pilot-injection energy is released before main injection starts.

Despite the additional pilot mass, the trend in the ignition delay is not consistent when the pilot mass is increased. Moreover, it can be seen that it is reduced at 12mg/st. Larger pilot masses would be needed to better understand the hypothesis that more pilot mass reduces the ignition delay. In the case of a shorter ignition delay, more time is available for the combustion of the pilot before the main injection, given a constant injection separation. The additional energy released from the pilot was found to have an effect on main injection and is further described in [51].

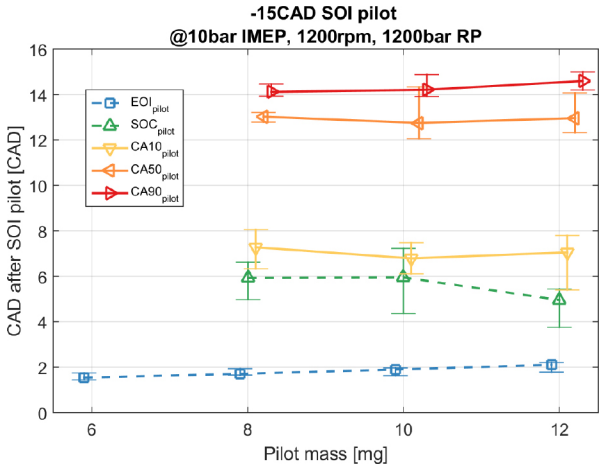


Figure 11. CAD after SOI of pilot-injection of EOI, SOC, CA10, CA50, CA90 at1200 rpm and 10bar IMEP; as a function of pilot-injection mass. Bars represent one standard deviation of the data set.

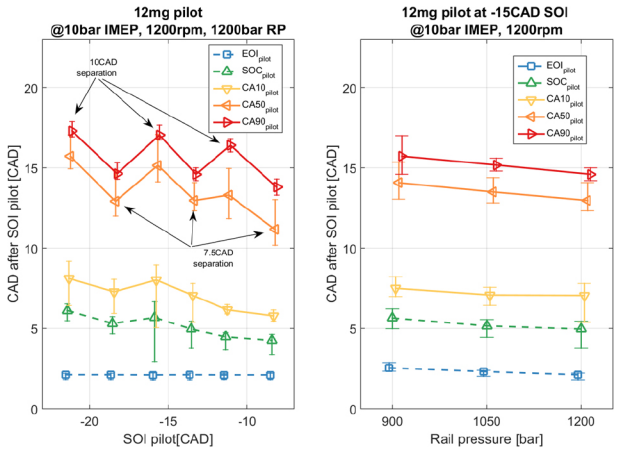


Figure 12. SOI, SOC, CA10, CA50 and CA90 as a function of SOI pilot (left) and rail pressure (right) at 10bar IMEP, 1200rpm. Bars represent one standard deviation of the data set.

The durations of the different pilot-injection combustion phases have been discussed as a function of the injected pilot mass. The next question is how they are affected by the start of pilot injection and by the rail pressure. In Figure 12, pilot-injection EOI, SOC, CA10, CA50 and CA90 after SOI are presented as a function of SOI and rail pressure. Results show that later injection reduces ignition delay, increasing the premixed combustion and the total heat that can be released before main injection. The saw-tooth shape in CA50 and CA90 is due to overlap of the pilot-injection and main-injection heat release. The lower values correspond to 7.5 CAD injection separation, and the higher to 10 CAD injection separation. For shorter separations, less heat can be released before main injection and therefore CA50 and CA90 advance. However, the global trend is a reduction in the difference between CA10 and CA50. The difference between CA50 and CA90 remains constant. Furthermore, the SOC and CA10 lines are parallel. This indicates that the premixed combustion duration is similar in all cases; it comprises 50% of the heat release of pilot injection before main injection.

A further question is whether the same results are obtained at different loads and engine speeds. Figure 13 presents the results of combustion timing parameters SOI, SOC, CA10, CA50 and CA90 of pilot-injection as a function of load at 1200 rpm and as a function of engine speed at 10 bar IMEP. In both cases, 12mg/st pilot is injected at -15 CAD SOI.

For increasing loads, rail pressure is increased accordingly, therefore there is a reduction in injection duration. It is observed that ignition delay and CA10-SOI remain constant. With a reduction at 15bar IMEP, probably due to the higher chamber temperature, CA50 and CA90 decrease more than the reduction in the ignition delay. This indicates that more heat is released during the fast, premixed combustion phase due to the higher temperature at higher loads.

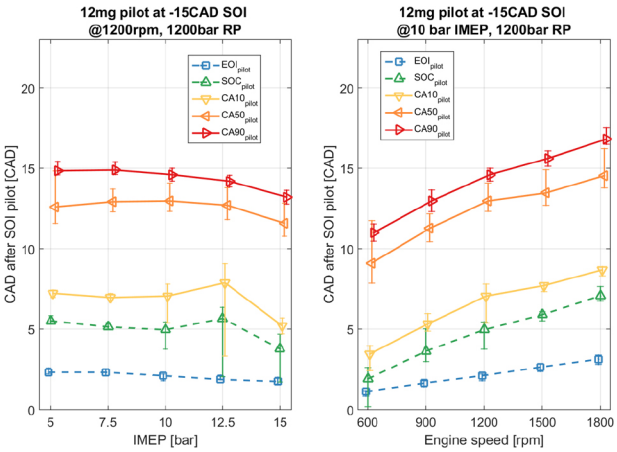


Figure 13. SOI, SOC, CA10, CA50 and CA90 as a function of load (left) and engine speed (right). Bars represent one standard deviation of the data set.

Looking at engine speed, the increase in injection duration corresponds to the relationship between CAD and time. Ignition delay follows the same increase which means that it is constant with time. However, CA10 is parallel with the ignition delay. The reason is an increase in the premixed combustion due to the higher temperature and turbulence. CA50 and CA90 are parallel with CA10. From this, it can be derived that diffusive combustion is constant with time despite the difference in engine speed.

## *Effect of Previous Cycle on Pilot Combustion*

Studies in HCCI combustion stability have shown that a preceding injection can affect autoignition and combustion of the following injection [52]. Depending on the initial inlet temperature at inlet valve closing (IVC), combustion can result in steady and stable

behaviour, but also in an oscillating combustion due to the preceding cycle combustion efficiency. An initial low IVC temperature results in the absence of autoignition in that cycle. The unburned fuel and residual gases modify the chamber conditions in the next cycle. This results in a lower ignition delay and the effect is a complete and early combustion. In the next cycle, there is no fuel from the preceding combustion, resulting in longer ignition delay, late combustion and low combustion efficiency. This loop starts again, resulting in the oscillating behaviour.

In this section the effect of previous cycle residuals on pilot combustion is discussed. To this end, the effect of first cycle main combustion efficiency on the second cycle pilot ignition delay is investigated.

The combustion efficiency was computed using the ratio between the AHR and the chemical energy content of the estimated injected mass.

The low combustion efficiency is explained by the bias in the estimated mass.

The results are presented in Figure 14:

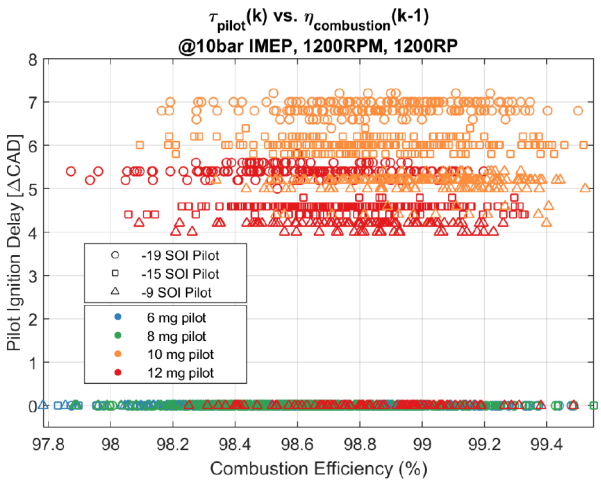


Figure 14. Pilot ignition delay at cycle 'k' vs. combustion efficiency at cycle 'k-1' at 10bar IMEP, 1200RPM and 1200bar Rail pressure for different SOI pilot and pilot masses. 0CAD ignition delay refers to cycles for which the pilot did not autoignite.

From this plot, it can be deduced that the preceding cycle combustion efficiency is less important for the following pilot ignition delay than the conditions at SOI. An ANCOVA analysis confirmed that the significance level in the covariance of the preceding cycle combustion efficiency was 0.56, much larger than the acceptable threshold of 0.05 in the p-value that is generally used. The ANCOVA analysis also confirmed that the difference in the mean for the different SOI of pilot injection was significant at 0.0006. ANCOVA analysis was performed for the various operating conditions. In all cases, the SOI for pilot injection was more significant than the combustion efficiency from the preceding cycle.

## CONCLUSIONS

Small pilot-injection autoignition and combustion were investigated using three pilot-injection parameters i.e. pilot-injection mass, pilot start of injection and rail pressure. Investigations were performed at different engine loads, engine speeds.

Autoignition of pilot injections under or equal to 6 mg/st was never achieved before the main injection. The cycle-to-cycle variations in the pilot autoignition are due to the individual cylinder chamber characteristics and injector-to-injector variations. The cycle-to-cycle variations are reduced with greater pilot mass, higher rail pressures and higher chamber temperature.

A minimum rail pressure is necessary to ensure pilot-injection autoignition. Retarding the SOI of the pilot enhances the robustness of pilot-injection autoignition.

The heat released from pilot combustion is a non-linear function of the pilot mass. The combustion efficiency of pilot injection increases with the injected pilot mass.

Higher load was found to decrease pilot ignition delay as more time for pilot combustion is available before main injection, resulting in more heat released. Lower engine speed also increases the available time for pilot combustion but this also increases the pilot ignition delay.

The pilot-injection ignition delay and pilot-combustion duration are reduced when the pilot SOI is retarded. The effect of pilot SOI on pilot-ignition delay was found to be more significant than the pilot mass.

The pilot-ignition delay has a negative linear relationship with increasing rail pressures. For higher rail pressures, the injection on-time and pilot ignition delay are shorter. The rail pressure was found not to have a significant effect on the duration of the pilot combustion.

The premixed combustion is constant in CAD domain and finishes 2 CAD after CA10 of pilot combustion. During premixed combustion, most of the pilot mass was burnt and diffusive combustion before main injection was only obtained at high engine load, high engine speed and large pilot masses.

The remaining residuals from combustion of the first cycle were not found to have a significant effect on pilot autoignition or pilot ignition delay of the second cycle.

## REFERENCES


1. Steffen, T., Stobart, R., and Yang, Z., "Challenges and Potential of Intra-Cycle Combustion Control for Direct Injection Diesel Engines," SAE Technical Paper 2012-01-1158, 2012, doi:10.4271/2012-01-1158.
2. Hellstrom, E., Larimore, J., Jade, S., Stefanopoulou, A.G., and Jiang, L., "Reducing cyclic variability while regulating combustion phasing in a four-cylinder HCCI engine," *IEEE Trans. Control Syst. Technol.* 22(3):1190-1197, 2014, doi:10.1109/TCST.2013.2271355.
3. Olsson, J., Tunestål, P., and Johansson, B., "Closed-Loop Control of an HCCI Engine," SAE Technical Paper 2001-01-1031, 2001, doi:10.4271/2001-01-1031.
4. Manente, V., Gasoline Partially Premixed Combustion An Advanced Internal Combustion Engine Concept Aimed to High Efficiency, Low Emissions and Low Acoustic Noise in the Whole Load Range, 2010.
5. Chiang, C.J. and Stefanopoulou, A.G., "Sensitivity Analysis of Combustion Timing and Duration of Homogeneous Charge Compression Ignition ( HCCI ) Engines," Proc. 2006 Am. Control Conf. 1857-1862, 2006, doi:10.1109/ACC.2006.1656490.
6. Kolbeck, A., "Closed Loop Combustion Control - Enabler of Future Refined Engine Performance Regarding Power, Efficiency, Emissions & NVH under Stringent Governmental Regulations," SAE Technical Paper 2011-24-0171, 2011, doi:10.4271/2011-24-0171.
7. Zander, C.-G., Tunestål, P., Stenlåås, O., and Johansson, B., "In-Cycle Closed Loop Control of the Fuel Injection on a 1-Cylinder Heavy Duty CI-Engine," ASME 2010 Internal Combustion Engine Division Fall Technical Conference, ASME, ISBN 978-0-7918-4944-6: 405-414, 2010, doi:10.1115/ICEF2010-35100.
8. Muric, K., Stenlaas, O., Tunestal, P., and Johansson, B., "A Study on In-Cycle Control of NOx Using Injection Strategy with a Fast Cylinder Pressure Based Emission Model as Feedback," SAE Technical Paper 2013-01-2603, 2013, doi:10.4271/2013-01-2603.
9. Saracino, R., Gaballo, M., Mannal, S., Motz, S. et al., "Cylinder Pressure-Based Closed Loop Combustion Control: A Valid Support to Fulfill Current and Future Requirements of Diesel Powertrain Systems," SAE Technical Paper 2015-24-2423, 2015, doi:10.4271/2015-24-2423.
10. Manente, V., Johansson, B., Tunestal, P., and Cannella, W., "Influence of Inlet Pressure, EGR, Combustion Phasing, Speed and Pilot Ratio on High Load Gasoline Partially Premixed Combustion," SAE Technical Paper 2010-01-1471, 2010, doi:10.4271/2010-01-1471.
11. Ryu, K., "Effects of pilot injection pressure on the combustion and emissions characteristics in a diesel engine using biodiesel-CNG dual fuel," *Energy Convers. Manag.*, 2013, doi:10.1016/j.enconman.2013.07.085.
12. Huang, H., Liu, Q., Yang, R., Zhu, T., Zhao, R., and Wang, Y., "Investigation on the effects of pilot injection on low temperature combustion in high-speed diesel engine fueled with n-butanol diesel blends," *Energy Convers. Manag.*, 2015, doi:10.1016/j.enconman.2015.10.031.
13. Wang, Z., Zhao, Z., Wang, D., Tan, M., Han, Y., Liu, Z., and Dou, H., "Impact of pilot diesel ignition mode on combustion and emissions characteristics of a diesel/natural gas dual fuel heavy-duty engine," *Fuel*, 2016, doi:10.1016/j.fuel.2015.11.077.
14. Torregrosa, A.J., Broatch, A., García, A., and Mónico, L.F., "Sensitivity of combustion noise and NOx and soot emissions to pilot injection in PCCI Diesel engines," *Appl. Energy*, 2013, doi:10.1016/j.apenergy.2012.11.040.
15. Carlucci, P., Ficarella, A., and Laforgia, D., "Effects of Pilot Injection Parameters on Combustion for Common Rail Diesel Engines," SAE Technical Paper 2003-01-0700, 2003, doi:10.4271/2003-01-0700.
16. Cheng, X., Chen, L., Yan, F., Hong, G. et al., "Investigations of Split Injection Strategies for the Improvement of Combustion and Soot Emissions Characteristics Based On the Two-Color Method in a Heavy-Duty Diesel Engine," SAE Technical Paper 2013-01-2523, 2013, doi:10.4271/2013-01-2523.
17. Lee, J., Jeon, J., Park, J., and Bae, C., "Effect of Multiple Injection Strategies on Emission and Combustion Characteristics in a Single Cylinder Direct-Injection Optical Engine," SAE Technical Paper 2009-01-1354, 2009, doi:10.4271/2009-01-1354.
18. Mingfa, Y., Hu, W., Zunqing, Z., and Yan, Y., "Experimental Study of Multiple Injections and Coupling Effects of Multi-Injection and EGR in a HD Diesel Engine," SAE Technical Paper 2009-01-2807, 2009, doi:10.4271/2009-01-2807.
19. Tanaka, T., Ando, A., and Ishizaka, K., "Study on pilot injection of DI diesel engine using common-rail injection system," *JSAE Rev.* 23(3):297-302, 2002, doi:10.1016/S0389-4304(02)00195-9.
20. Badami, M., Mallamo, F., Millo, F., and Rossi, E., "Influence of Multiple Injection Strategies on Emissions, Combustion Noise and BSFC of a DI Common Rail Diesel Engine," SAE Technical Paper 2002-01-0503, 2002, doi:10.4271/2002-01-0503.
21. D'Ambrosio, S., Ferrari, A., D'Ambrosio, S., and Ferrari, A., "Potential of double pilot injection strategies optimized with the design of experiments procedure to improve diesel engine emissions and performance," *Appl. Energy* 155:918-932, 2015, doi:10.1016/j.apenergy.2015.06.050.
22. Manente, V., Johansson, B., Tunestal, P., and Cannella, W., "Influence of Inlet Pressure, EGR, Combustion Phasing, Speed and Pilot Ratio on High Load Gasoline Partially Premixed Combustion," SAE Technical Paper 2010-01-1471, 2010, doi:10.4271/2010-01-1471.
23. Mendez, S. and Thirouard, B., "Using Multiple Injection Strategies in Diesel Combustion: Potential to Improve Emissions, Noise and Fuel Economy Trade-Off in Low CR Engines," *SAE Int. J. Fuels Lubr.* 1(1):662-674, 2009, doi:10.4271/2008-01-1329.
24. Badami, M., Millo, F., and D'Amato, D., "Experimental Investigation on Soot and NOx Formation in a DI Common Rail Diesel Engine with Pilot Injection," SAE Technical Paper 2001-01-0657, 2001, doi:10.4271/2001-01-0657.
25. Okude, K., Mori, K., Shiino, S., Yamada, K. et al., "Effects of Multiple Injections on Diesel Emission and Combustion Characteristics," SAE Technical Paper 2007-01-4178, 2007, doi:10.4271/2007-01-4178.
26. Muric, K., Stenlaas, O., Tunestal, P., and Johansson, B., "A Study on In-Cycle Control of NOx Using Injection Strategy with a Fast Cylinder Pressure Based Emission Model as Feedback," SAE Technical Paper 2013-01-2603, 2013, doi:10.4271/2013-01-2603.
27. Heywood J.B., "Internal Combustion Engines Fundamentals," 6th ed., McGraw Hill Education, New York, ISBN 0-07-100499-8, 1988.
28. Groendyk, M. and Rothamer, D., "Effects of Fuel Physical Properties on Auto-Ignition Characteristics in a Heavy Duty Compression Ignition Engine," *SAE Int. J. Fuels Lubr.* 8(1):200-213, 2015, doi:10.4271/2015-01-0952.
29. Siebers, D., "Liquid-Phase Fuel Penetration in Diesel Sprays," SAE Technical Paper 980809, 1998, doi:10.4271/980809.
30. Dhuchakallaya, I. and Watkins, A.P., "Auto-ignition of diesel spray using the PDF-Eddy Break-Up model," *Appl. Math. Model.*, 2010, doi:10.1016/j.apm.2009.09.019.
31. Sazhin, S. S., Feng, G., Heikal, M. R., Goldfarb, I., Goldshtein, V. and Kuzmenko, G., "Thermal ignition analysis of a monodisperse spray with radiation," *Combust. Flame* 684-701.
32. Zheng, J., Miller, D., and Cernansky, N., "A Global Reaction Model for the HCCI Combustion Process," SAE Technical Paper 2004-01-2950, 2004, doi:10.4271/2004-01-2950.
33. Jung, D. and Assanis, D., "Multi-Zone DI Diesel Spray Combustion Model for Cycle Simulation Studies of Engine Performance and Emissions," SAE Technical Paper 2001-01-1246, 2001, doi:10.4271/2001-01-1246.
34. Finesso, R. and Spessa, E., "Ignition delay prediction of multiple injections in diesel engines," *Fuel* 119:170-190, 2014, doi:10.1016/j.fuel.2013.11.040.
35. Dec, J., "A Conceptual Model of DI Diesel Combustion Based on Laser-Sheet Imaging*," SAE Technical Paper 970873, 1997, doi:10.4271/970873.
36. Tunestål, P., "Self-tuning gross heat release computation for internal combustion engines," *Control Eng. Pract.* 17(4):518-524, 2009, doi:10.1016/j.conengprac.2008.09.012.
37. Johansson, T. and Stenlåås, O., "Heat Release Based Virtual Combustion Sensor Signal Bias Sensitivity," SAE Techcnical Paper 2017-01-0789, 2017, doi:10.4271/2017-01-0789.
38. Tunestål, P., "TDC Offset Estimation from Motored Cylinder Pressure Data based on Heat Release Shaping," *Oil Gas Sci. Technol. - Rev. IFP Energies Nouv.* 66(4):705-716, 2011, doi:10.2516/ogst/2011144.
39. Woschni, G., "A Universally Applicable Equation for the Instantaneous Heat Transfer Coefficient in the Internal Combustion Engine," SAE Technical Paper 670931, 1967, doi:10.4271/670931.
40. Oh, S., Min, K., and Sunwoo, M., "Real-time start of a combustion detection algorithm using initial heat release for direct injection diesel engines," *Appl. Therm. Eng.*, 2015, doi:10.1016/j.applthermaleng.2015.05.079.
41. Yoon, M., Lee, K., Sunwoo, M., and Oh, B., "Cylinder Pressure Based Combustion Phasing Control of a CRDI Diesel Engine," SAE Technical Paper 2007-01-0772, 2007, doi:10.4271/2007-01-0772.

42. Katrašnik, T., Trenc, F., and Oprešnik, S.R., "A New Criterion to Determine the Start of Combustion in Diesel Engines," *J. Eng. Gas Turbines Power* 128(4):928, 2006, doi:10.1115/1.2179471.
43. Catania, A.E., Misul, D., Spessa, E., and Vassallo, A., "A Diagnostic Tool for the Analysis of Heat Release, Flame Propagation Parameters and NO Formation in SI Engines(S.I. Engines, Combustion Diagnostics)," *Int. Symp. Diagnostics Model. Combust. Intern. Combust. Engines* 2004(6):471-486, 2004.
44. Baratta, M., Catania, A.E., Ferrari, A., Finesso, R., and Spessa, E., "Premixed-Diffusive Multizone Model for Combustion Diagnostics in Conventional and PCCI Diesel Engines," *J. Eng. Gas Turbines Power* 133(10):102801, 2011, doi:10.1115/1.4003048.
45. Klein, P., Grüter, R., and Loffeld, O., "Real-Time Estimation of the Exhaust Gas Recirculation Ratio Based on Cylinder Pressure Signals," SAE Technical Paper 2007-01-0493, 2007, doi:10.4271/2007-01-0493.
46. Zhong, L., Singh, I., Han, J., Lai, M. et al., "Effect of Cycle-to-Cycle Variation in the Injection Pressure in a Common Rail Diesel Injection System on Engine Performance," SAE Technical Paper 2003-01-0699, 2003, doi:10.4271/2003-01-0699.
47. Dernotte, J., Hespel, C., Foucher, F., Houillé, S., and Mounaïm-rousselle, C., "Influence of physical fuel properties on the injection rate in a Diesel injector," *Fuel* 96:153-160, 2012, doi:10.1016/j.fuel.2011.11.073.
48. Yuan, W., Hansen, A.C., Tat, M.E., Gerpen, Van J.H., Tan, Z., Tat, M.E., and Gerpen, Van J.H., "Spray, ignition and combustion modeling of biodiesel fuels for investigating NOx emissions," *Trans. ASAE* 48(3):933-939.
49. Xu, M., Nishida, K., and Hiroyasu, H., "A Practical Calculation Method for Injection Pressure and Spray Penetration in Diesel Engines," SAE Technical Paper 920624, 1992, doi:10.4271/920624.
50. Teng, H., McCandless, J., and Schneyer, J., "Compression Ignition Delay (Physical + Chemical) of Dimethyl Ether - An Alternative Fuel for Compression-Ignition Engines," SAE Technical Paper 2003-01-0759, 2003, doi:10.4271/2003-01-0759.
51. Jorques Moreno, C., Stenlåås, O., and Tunestål, P., "Influence of Small Pilot on Main Injection in a Heavy Duty Diesel Engine," SAE Techcnical Paper 2017-01-0708, 2017, doi:10.4271/2017-01-0708.
52. Erlandsson, O., "Thermodynamic Simulation of HCCI Engine Systems," Lund Institute of Technology, Lund, ISBN 9162854275, 2002.


## CONTACT INFORMATION

moreno.carlos.jorques@scania.com

## ACKNOWLEDGEMENTS

The authors would like to acknowledge the Swedish Energy Agency for funding the research project, the Competence Center for the Combustion Processes at Lund University, LTH, and Scania CV AB for the test and equipment facilities. Gabriel Ingesson and Lianhao Yin are acknowledged for their support and valuable feedback.

## DEFINITIONS/ABBREVIATIONS

**CA10** - Crank angle at which 10% of the total accumulated heat release is reached

**CA50** - Crank angle at which 50% of the total accumulated heat release is reached

**CA90** - Crank angle at which 90% of the total accumulated heat release is reached

**CAD** - Crank angle degree

**DBCC** - Combustion Duration Before Centre of Combustion

**EGR** - Exhaust gas recirculation

**HCCI** - Homogeneous Charge Compression Ignition

**AHR** - Accumulated heat release

**HR** - Heat release rate

**PPC** - Partially Premixed Combustion

**PRR** - Pressure rise rate

**IMEP** - Indicated mean effective pressure

**NOx** - Nitrogen oxides

**UHC** - Unburned Hydrocarbons

**RP** - Rail pressure

**RPM** - Revolutions per minute

**SOI** - Start of injection

**EOI** - End of injection

**SOC** - Start of combustion

**EOC** - End of combustion

**TDC** - Top dead centre